ELSEVIER

Engineering Analysis with Boundary Elements 30 (2006) 963–970

ENGINEERING ANALYSIS with BOUNDARY ELEMENTS

www.elsevier.com/locate/enganabound

A 2-D model that accounts for 3-D fringing in MEMS devices

Krishnan Suresh*, Murari Sinha

Department of Mechanical Engineering, University of Wisconsin—Madison, 1513 University Avenue, USA

Received 29 December 2005; accepted 3 March 2006

Abstract

MEMS devices such as comb drives and rotary drives are geometrically simple in that each of the components may be represented as a 'sweep' of a 2-D cross-section through a given height. This simplicity leads to simpler CAD requirements, geometric robustness, faster visualization, etc. Further, 3-D electrostatic simulation may be simplified to a 2-D problem over the cross-section if one neglects 3-D fringing. Such 2-D simulations provide a quick feedback to the designer on various parameters such as capacitance and electrostatic forces.

However, as is well known, 3-D simulations cannot be avoided if fringing is significant, or when these devices need to be fully optimized. Such 3-D simulations unfortunately involve constructing the full 3-D geometry, volume/surface mesh, etc.

In this paper, we demonstrate that one can pose and solve a 2-D problem that accounts for 3-D fringing. The proposed technique does not require the construction of the 3-D CAD model or surface/volume mesh. Instead, the 3-D electrostatics problem is collapsed to 2-D via a novel dimensional reduction method. Once the 2-D problem is solved, the full 3-D field and associated charges/forces can be recovered, as a post-processing step. The simplicity and computational efficiency of the technique lends itself well to parametric study and design optimization.

Keywords: MEMS; Dimensional reduction; Fringing; CAD

1. Introduction

Current design/simulations challenges in MEMS include shape optimization [1–3], multi-physics problems [4–7], non-linear problems [4,5] and development of low-order models [8–10]. However, underlying all of these challenges is the basic 3-D electrostatic simulation problem that needs to be solved as efficiently as possible. Thus, despite the availability of commercial packages that address electrostatic simulation, for example, see [11–13], 3-D electrostatic simulation continues to generate interest among researchers, and new techniques are constantly being developed [14–16].

The objective of this paper is to provide a new approach to 3-D electrostatic simulation that can potentially impact all of the design/simulation challenges mentioned above. The concept proposed here is that of dimensional reduction where a spatial variable, specifically the thickness variable, is eliminated prior to computational analysis. Thus, 3-D modeling is unnecessary, and a complete 3-D simulation is possible from a 2-D cross-sectional data (with height as a design parameter).

Furthermore, when the device is thin, the proposed dimensional reduction method avoids the pitfalls faced by full 3-D finite-element and boundary-element techniques that require special formulations [17].

1.1. Problem formulation

Let the MEMS device consist of numerous components whose cross-sections are in the xy plane, and are denoted by d^{α}. For example, Fig. 1 illustrates two cross-sections d^1 and d^2.

For simplicity, we assume that the heights of all components range from $-H$ to H; differing heights are not addressed here. The corresponding 3-D components obtained by sweeping the cross-sections d^{α} from $-H$ to H are denoted D^{α} (Fig. 2).

*Corresponding author.
E-mail addresses: suresh@engr.wisc.edu (K. Suresh), msinha1@engr.wisc.edu (M. Sinha).

0955-7997/$ - see front matter © 2006 Elsevier Ltd. All rights reserved.
doi:10.1016/j.enganabound.2006.07.007

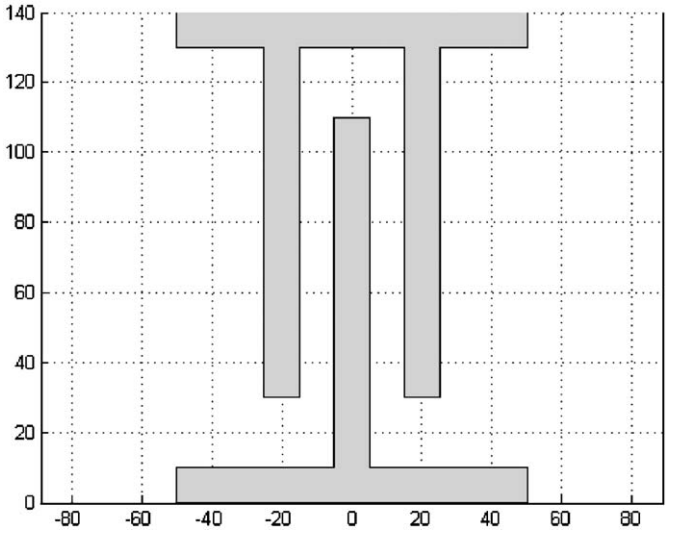

Fig. 1. The 2-D cross-section profiles.

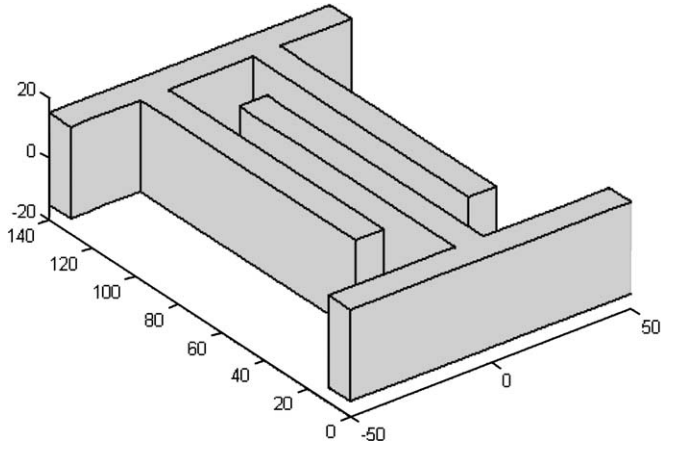

Fig. 2. The 3-D geometry.

We assume that the components are enclosed in 3-D space that is open in all directions except for the presence of a ground plane at $z = -z^g$ beneath the devices.[1] Further, let a voltage $\hat{v}^\alpha$ be applied to the component D^α. Thus the 3-D electrostatic problem over the 3-D space Ω surrounding the 3-D components is

$$\begin{aligned} &\nabla^2 U(x,y,z) = 0 \text{ in } \Omega, \\ &U = \hat{v}^\alpha \text{ on } \partial D^\alpha, \\ &U(x,y,-z^g) = 0, \\ &U(p,z) \to 0 \text{ as } p \to \infty, \text{ or, } z \to \infty. \end{aligned} \tag{1}$$

Existing 3-D simulation techniques disregard the special geometric structure underlying the domain Ω and seek solutions either by (a) converting the above equation into an integral form for boundary element analysis [18] or (b) convert it into a weak form (below) for finite-element analysis (FEA) [19].

In passing, we note that the 2-D formulation of Eq. (1) is simply

$$\begin{aligned} &\nabla^2 U(x,y) = 0 \text{ in } \omega, \\ &U = \hat{v}^\alpha \text{ on } \partial d^\alpha, \\ &U(p) \to 0 \text{ as } p \to \infty, \end{aligned} \tag{2}$$

where ω is the 2-D space surrounding the device. Observe that the boundary conditions in the z direction play no role in the above formulation, leading to a possible discrepancy due to fringing effects.

In this paper, we shall consider the dimensional reduction of Eq. (1). Dimensional reduction techniques are popular in structural mechanics where dimensionally reduced models, for example, plate and shell models, have been successfully used for many decades now [20,21]. Such models exploit the fact that plates and shells may be expressed as a lower-dimensional cross-section plus a thickness.

Direct application of such dimensional reduction techniques to MEMS is faulty for the following reason: although individual MEMS components may be expressed as cross-section plus thickness, the free space surrounding the components (where simulation needs to be carried out) cannot. Thus, classic dimensional reduction techniques do not apply. New strategies are needed, and pursued here.

In particular, we will find it most convenient to start with the 3-D weak formulation of Eq. (1):

$$\begin{cases} \text{Find } U \in \mathscr{U}(\Omega) \text{ such that} \\ \int_\Omega \nabla V^{\mathrm{T}} c \nabla U \, \mathrm{d}\Omega = 0 \\ \forall\ V \in \mathscr{V}(\Omega), \end{cases} \tag{3}$$

where the trial and test spaces are defined as follows:

$$\mathscr{U}(\Omega) = \left\{ \begin{array}{l} U \in \mathbf{H}^1(\Omega);\ \ U = \hat{v}^\alpha \text{ on } \partial D^\alpha;\ U(x,y,-z^g) = 0 \\ U(p,z) \to 0 \text{ as } p \to \infty, \text{ or, } z \to \infty \end{array} \right\} \tag{4}$$

and

$$\mathscr{V}(\Omega) = \left\{ \begin{array}{l} V \in \mathbf{H}^1(\Omega);\ \ V = 0 \text{ on } \partial D^\alpha;\ \ V(x,y,-z^g) = 0 \\ V(p,z) \to 0 \text{ as } p \to \infty, \text{ or, } z \to \infty \end{array} \right\}. \tag{5}$$

2. Dimensional reduction

Our objective here is to exploit the special geometric structure underlying Ω to solve the above 3-D problem while minimizing the computational and infrastructure requirements. To meet this objective, we view the region Ω

[1] The problem formulation and ensuing theory can be modified if the enclosing space is of a different structure (say insulated in some directions).

as consisting of three quasi-disjoint regions:

$$\Omega(x,y,z) = \bigcup \begin{cases} \Omega^1 = \Omega(x,y,z<-H), \\ \Omega^2 = \Omega(x,y,-H<z<H), \\ \Omega^3 = \Omega(x,y,z>H). \end{cases}$$

Now observe that each of the above regions may be expressed as a sweep of a corresponding cross-section through appropriate (possible infinite) heights; these cross-sections are

$$\begin{aligned} &\omega^1 \equiv \omega \cup \left(\bigcup_\alpha d^\alpha \right), \\ &\omega^2 \equiv \omega, \\ &\omega^3 \equiv \omega^1, \end{aligned} \tag{6}$$

where ω is the 2-D space surrounding the devices d^α. Given the space decomposition, we split the unknown field $U(x, y, z)$ into three corresponding fields:

$$U(x,y,z) = \begin{cases} U^1(x,y,z) & \text{for } z<-H, \\ U^2(x,y,z) & \text{for } -H<z<H, \\ U^3(x,y,z) & \text{for } z>H. \end{cases}$$

In this section, we shall demonstrate that the spatial variable z can be eliminated from each of the three fields while maintaining the required continuity between them, reducing the 3-D problem to a 2-D problem.

2.1. Solution space description

The three fields U^1, U^2 and U^3 defined above must satisfy the Laplace equation in their respective domains, i.e., we have

$$\nabla^2 U^i(x,y,z) = 0 \text{ in } \Omega^i.$$

We now need to specify the boundary conditions for each of these fields. Consider U^1: the only relevant boundary conditions that may be extracted from Eq. (4) are

$$\begin{aligned} &U^1(x,y,-H) = \hat{v}^\alpha \text{ on } d^\alpha(-H), \\ &U^1(x,y,-z^g) = 0, \\ &U^1(p,z) \to 0 \text{ as } p \to \infty, \end{aligned}$$

where one interprets $d^\alpha(-H)$ as the translation of the 2-D region d^α to $z=-H$. The above equation states that the field U^1 must take the value of the applied voltage on the bottom surface of the components, go to zero on the ground plane and go to zero as points $p=(x,y)$ far from the origin. Similarly, the boundary conditions on U^2 are

$$\begin{aligned} &U^2(x,y,z) = \hat{v}^\alpha \text{ on } \partial d^\alpha(-H<z<H), \\ &U^2(p,z) \to 0 \text{ as } p \to \infty. \end{aligned}$$

Finally, the boundary conditions on U^3 are

$$\begin{aligned} &U^3(x,y,H) = \hat{v}^\alpha \text{ on } d^\alpha(H), \\ &U^3(p,z) \to 0 \text{ as } p \to \infty, \text{ or, } z \to \infty. \end{aligned}$$

The above boundary conditions essentially define the subspaces within which one must seek solutions for $U^i(x,y,z)$; $i=1,2,3$:

$$\mathscr{U}^1(\Omega^1) = \left\{ \begin{array}{l} U^1 \in \mathbf{H}^1(\Omega^1); \\ U^1(x,y,-H) = \hat{v}^\alpha \text{ on } d^\alpha(-H), \\ U^1(x,y,-z^g) = 0, \\ U^1(p,z) \to 0 \text{ as } p \to \infty \end{array} \right\} \tag{7}$$

$$\mathscr{U}^2(\Omega^2) = \left\{ \begin{array}{l} U^2 \in \mathbf{H}^1(\Omega^2); \\ U^2(x,y,z) = \hat{v}^\alpha \text{ on } \partial d^\alpha(-H<z<H), \\ U^2(p,z) \to 0 \text{ as } p \to \infty \end{array} \right\} \tag{8}$$

$$\mathscr{U}^3(\Omega^3) = \left\{ \begin{array}{l} U^3 \in \mathbf{H}^1(\Omega^3); \\ U^3(x,y,H) = \hat{v}^\alpha \text{ on } d^\alpha(H), \\ U^3(p,z) \to 0 \text{ as } p \to \infty, \text{ or, } z \to \infty \end{array} \right\} \tag{9}$$

The corresponding test spaces $\mathscr{W}^i(\Omega^i)$ needed in the weak formulation may be defined by replacing $\hat{v}^\alpha$ by 0 in the above equation.

Observe that in addition to satisfying the boundary conditions, the fields must satisfy continuity conditions along the interfaces of Ω^1 and Ω^2, and Ω^2 and Ω^3. Classic continuity requirements between sub-domains need to be imposed, and these are

$$\text{On the interface of } \Omega^1 \text{ and } \Omega^2 \begin{cases} U^1 = U^2, \\ \frac{\partial U^2}{\partial z} = \frac{\partial U^1}{\partial z}, \end{cases}$$

$$\text{On the interface of } \Omega^1 \text{ and } \Omega^3 \begin{cases} U^3 = U^2, \\ \frac{\partial U^2}{\partial z} = \frac{\partial U^1}{\partial z}. \end{cases}$$

Observe that the interface of Ω^1 and Ω^2 may be represented as $\omega(-H)$ where one interprets $\omega(-H)$ as the translation of the 2-D space ω to $z=-H$, so on. For simplicity, we view the Dirichlet continuity conditions above as constraints on Ω^1 and Ω^3 while the Neumann (flux) constraints are viewed as constraints on Ω^2 (and later captured by adding appropriate terms to the variational statement). Thus, we have

$$\left. \begin{array}{l} U^1 = U^2 \\ \frac{\partial U^2}{\partial z} = \frac{\partial U^1}{\partial z} \end{array} \right\} \text{ on } \omega(-H),$$

$$\left. \begin{array}{l} U^3 = U^2 \\ \frac{\partial U^2}{\partial z} = \frac{\partial U^3}{\partial z} \end{array} \right\} \text{ on } \omega(+H).$$

One may now restate the 3-D electrostatic problem posed in Eq. (3) as

$$\begin{cases} \text{Find } U^i \in \mathscr{U}^i(\Omega^i),\ i=1,2,3 \text{ such that} \\ U^1 = U^2 \text{ on } \omega(-H); \quad U^3 = U^2 \text{ on } \omega(H) \\ \left[\sum_{i=1}^{3} \int_{\Omega^i} (\nabla V^i)^{\mathrm{T}} \nabla U^i \,\mathrm{d}\Omega + \int_{\omega(-H)} V^2 \frac{\partial U^1}{\partial z}\,\mathrm{d}\omega \right. \\ \qquad \left. - \int_{\omega(H)} V^2 \frac{\partial U^3}{\partial z}\,\mathrm{d}\omega\right] = 0 \\ \forall\ V^i \in \mathscr{V}^i(\Omega^i), i=1,2,3, \text{ where} \\ V^1 = 0 \text{ on } \omega(-H); \quad V^3 = 0 \text{ on } \omega(H). \end{cases} \tag{10}$$

We have included both the Dirichlet and Neumann continuity constraints into the above formulation.

2.2. The three stages of reduction

We now consider the dimensional reduction of Eq. (10) by eliminating the z variable as follows. For convenience, we introduce non-dimensional entities ξ^i:

$$z = \begin{cases} -\frac{(z^g+H)}{2} + \xi^1 \frac{(z^g-H)}{2}; & z < -H \\ H\xi^2; & -H \leqslant z \leqslant H \\ \frac{2H}{1-\xi^3}; & z > H \end{cases} \tag{11}$$

where $-z^g$ is the location of the grounding plane below the MEMS device. The mapping is illustrated in Fig. 3. Observe that the infinite space in the $+z$ direction has been collapsed to a finite space via the third transformation in Eq. (11).

From Eq. (11), Jacobians are defined per:

$$\mathrm{d}z = J^i \,\mathrm{d}\xi^i; \quad J^1 = \frac{(z^g - H)}{2}; \quad J^2 = H; \quad J^3 = \frac{2H}{(1-\xi^3)^2} \tag{12}$$

and the inverse mapping is given by

$$\xi^1 = \frac{2z + (z^g + H)}{(z^g - H)}; \quad \xi^2 = \frac{z}{H}; \quad \xi^3 = \frac{-2H}{z} + 1. \tag{13}$$

The proposed dimensional reduction rests on seeking approximations of the form:

$$U^i(x,y,\xi^i) = \sum_{j=1}^{p} u_j^i(x,y) N_j(\xi^i). \tag{14}$$

This is now parallel to the dimensional reduction techniques used in plate and shell theories [22]. Further, we shall demonstrate later on that such representations yield highly accurate description of the 3-D field, where the parameter p controls the accuracy. Typical values for p range from 3 to 6. The choice of the shape functions $N_j(\xi)$ is also discussed in a later section. For now, we only require that these functions be linearly independent.

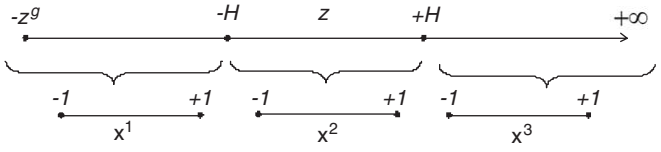

Fig. 3. Mapping of z to non-dimensional entities.

For brevity, we shall write Eq. (14) and its dual in a vector form:

$$\begin{aligned} U^i(x,y,z) &= \mathbf{N}^{\mathrm{T}}(\xi^i)\mathbf{u}^i(x,y), \\ V^i(x,y,z) &= \mathbf{N}^{\mathrm{T}}(\xi^i)\mathbf{v}^i(x,y), \end{aligned} \tag{15}$$

where

$$\mathbf{N}(\xi^i)^{\mathrm{T}} = \{\, N_1(\xi^i) \quad N_2(\xi^i) \quad \cdots \quad N_p(\xi^i) \,\},$$

$$\mathbf{u}^i(x,y)^{\mathrm{T}} = \{\, u_1^i(x,y) \quad u_2^i(x,y) \quad \cdots \quad u_p^i(x,y) \,\},$$

$$\mathbf{v}^i(x,y)^{\mathrm{T}} = \{\, v_1^i(x,y) \quad v_2^i(x,y) \quad \cdots \quad v_p^i(x,y) \,\}.$$

Our objective is now to transform the problem in Eq. (10) to an equivalent 2-D problem governing $\mathbf{u}^i(x,y)$. This is done in three stages:

Stage 1. Reduction of solution space

We shall first study the sub-space within which the fields $\mathbf{u}^i(x,y)$ must lie. Let us consider the space $\mathscr{U}^1(\Omega^1)$, defined in Eqs. (7)–(9). Direct substitution of Eq. (15) into Eq. (7), together with the mapping in Eq. (13) results in

$$U^1(\omega^1) = \left\{ \begin{array}{l} \mathbf{u}^1 = \left\{ u_1^1(x,y) \quad \cdots \quad u_{\mathrm{p}}^1(x,y) \right\} \in \mathbf{H}_p^1(\omega^1) \\ \mathbf{N}^{\mathrm{T}}(+1)\mathbf{u}^1(x,y) = \hat{v}^\alpha \text{ on } d^\alpha \\ \mathbf{N}^{\mathrm{T}}(-1)\mathbf{u}^1(x,y) = 0 \text{ on } d^\alpha \\ \mathbf{u}^1(p) \to 0 \text{ as } p \to \infty \end{array} \right\}. \tag{16}$$

Similar simplification of the sub-space $\mathscr{U}^2(\Omega^2)$ results in[2]

$$U^2(\omega^2) = \left\{ \begin{array}{l} \mathbf{u}^2 = \{\, u_1^2(x,y) \quad \ldots \quad u_{\mathrm{p}}^2(x,y) \,\} \in \mathbf{H}_{\mathrm{p}}^1(\omega^2) \\ \mathbf{N}^{\mathrm{T}}(\xi)\mathbf{u}^2(x,y) = \hat{v}^\alpha \text{ on } \partial d^\alpha(\xi) \\ \mathbf{u}^2(p) \to 0 \text{ as } p \to \infty \end{array} \right\}. \tag{17}$$

Finally, the sub-space $\mathscr{U}^3(\omega^3)$ is given by

$$\mathscr{U}^3(\omega^3) = \left\{ \begin{array}{l} \mathbf{u}^3 = \left\{ u_1^3(x,y) \quad \ldots \quad u_{\mathrm{p}}^3(x,y) \right\} \in \mathbf{H}_p^1(\omega^3) \\ \mathbf{N}^{\mathrm{T}}(-1)\mathbf{u}^3(x,y) = \hat{v}^\alpha \text{ on } d^\alpha \\ \mathbf{N}^{\mathrm{T}}(+1)\mathbf{u}^3(x,y) = 0 \\ \mathbf{u}^3(p) \to 0 \text{ as } p \to \infty \end{array} \right\}. \tag{18}$$

[2]The middle term needs to be simplified further before it can be used; the simplification depends on the shape function (see section on choice of shape functions).

Stage 2: Enforcing Dirichlet continuity

Now consider the Dirichlet continuity conditions in Eq. (10):

$$U^1 = U^2 \text{ on } \omega(-H),$$
$$U^3 = U^2 \text{ on } \omega(+H).$$

Direct substitution of Eq. (15) yields:

$$\mathbf{N}^{\mathrm{T}}(+1)\mathbf{u}^1(x,y) = \mathbf{N}^{\mathrm{T}}(-1)\mathbf{u}^2(x,y) \text{ on } \omega^2,$$
$$\mathbf{N}^{\mathrm{T}}(+1)\mathbf{u}^2(x,y) = \mathbf{N}^{\mathrm{T}}(-1)\mathbf{u}^3(x,y) \text{ on } \omega^2.$$

Stage 3: Reduction of variational term

Next consider the integral term in Eq. (10):

$$\sum_{i=1}^{3} \int_{\Omega^i} (\nabla V^i)^{\mathrm{T}} \nabla U^i \, \mathrm{d}\Omega = 0.$$

This may be expressed as

$$\sum_{i=1}^{3} \int_{\omega^i} \int_{-1}^{1} (\nabla V^i)^{\mathrm{T}} \nabla U^i J^i \, \mathrm{d}\xi^i = 0.$$

Observe from Eqs. (12) and (15) that

$$\nabla U^i = \begin{Bmatrix} \mathbf{N}^{\mathrm{T}}\mathbf{u}^i_{,x} \\ \mathbf{N}^{\mathrm{T}}\mathbf{u}^i_{,y} \\ \frac{1}{J^i}\mathbf{N}^{\mathrm{T}}_{,\xi}\mathbf{u}^i \end{Bmatrix}; \quad \nabla V^i = \begin{Bmatrix} \mathbf{N}^{\mathrm{T}}\mathbf{v}^i_{,x} \\ \mathbf{N}^{\mathrm{T}}\mathbf{v}^i_{,y} \\ \frac{1}{J^i}\mathbf{N}^{\mathrm{T}}_{,\xi}\mathbf{v}^i \end{Bmatrix}; \quad i = 1,2,3. \tag{19}$$

Substituting the above results in

$$\sum_{i=1}^{3} \int_{\omega^i} \left[\begin{Bmatrix} (\mathbf{v}^i_{,x})^{\mathrm{T}} & (\mathbf{v}^i_{,y})^{\mathrm{T}} & (\mathbf{v}^i)^{\mathrm{T}} \end{Bmatrix} \mathbf{C}^i \begin{Bmatrix} \mathbf{u}^i_{,x} \\ \mathbf{u}^i_{,y} \\ \mathbf{u}^i \end{Bmatrix} \right] \mathrm{d}\omega = 0,$$

where

$$[\mathbf{C}^i] = \int_{-1}^{1} \begin{bmatrix} \mathbf{N}\mathbf{N}^{\mathrm{T}} & 0 & 0 \\ 0 & \mathbf{N}\mathbf{N}^{\mathrm{T}} & 0 \\ 0 & 0 & \left(\frac{1}{J^i}\right)^2 \mathbf{N}_{,\xi}\mathbf{N}^{\mathrm{T}}_{,\xi} \end{bmatrix} J^i \, \mathrm{d}\xi. \tag{20}$$

Now consider the surface integrals in Eq. (10) that capture the Neumann continuity:

$$\int_{\omega(-H)} V^2 \frac{\partial U^1}{\partial z} \, \mathrm{d}\omega - \int_{\omega(H)} V^2 \frac{\partial U^3}{\partial z} \, \mathrm{d}\omega.$$

Substituting Eqs. (15) and (19), we have

$$\frac{1}{J^1} \int_{\omega} \mathbf{v}^2 \mathbf{N}(-1)\mathbf{N}^{\mathrm{T}}_{,\xi}(+1)\mathbf{u}^1 \, \mathrm{d}\omega - \frac{1}{J^3} \int_{\omega} \mathbf{v}^2 \mathbf{N}(+1)\mathbf{N}^{\mathrm{T}}_{,\xi}(-1)\mathbf{u}^3 \, \mathrm{d}\omega.$$

2.3. Summary of proposed methodology

In summary, the weak statement in Eq. (10), upon the approximation made in Eq. (15) may be reduced to the following 2-D vector problem involving the unknown fields $\mathbf{u}^i(x,y)$:

$$\left\{ \begin{array}{l} \text{Find } \mathbf{u}^i \in \mathscr{U}^i(\omega^i); \quad i = 1,2,3 \text{ such that} \\ \mathbf{N}^{\mathrm{T}}(+1)\mathbf{u}^1(x,y) = \mathbf{N}^{\mathrm{T}}(-1)\mathbf{u}^2(x,y) \text{ on } \omega^2, \\ \mathbf{N}^{\mathrm{T}}(+1)\mathbf{u}^2(x,y) = \mathbf{N}^{\mathrm{T}}(-1)\mathbf{u}^3(x,y) \text{ on } \omega^2, \\ \left\{ \begin{array}{l} \displaystyle\sum_{i=1}^{3} \int_{\omega^i} \left[\begin{Bmatrix} (\mathbf{v}^i_{,x})^{\mathrm{T}} & (\mathbf{v}^i_{,y})^{\mathrm{T}} & (\mathbf{v}^i)^{\mathrm{T}} \end{Bmatrix} \mathbf{C}^i \begin{Bmatrix} \mathbf{u}^i_{,x} \\ \mathbf{u}^i_{,y} \\ \mathbf{u}^i \end{Bmatrix} \right] \mathrm{d}\omega \\ \quad + \frac{1}{J^1} \int_{\omega} \mathbf{v}^2 \mathbf{N}(-1)\mathbf{N}^{\mathrm{T}}_{,\xi}(+1)\mathbf{u}^1 \, \mathrm{d}\omega \\ \quad - \frac{1}{J^3} \int_{\omega} \mathbf{v}^2 \mathbf{N}(+1)\mathbf{N}^{\mathrm{T}}_{,\xi}(-1)\mathbf{u}^3 \, \mathrm{d}\omega \end{array} \right\} = 0 \\ \forall \ \mathbf{v}^i \in \mathbf{V}^i(\omega^i); \quad i = 1,2,3, \quad \text{where} \\ \mathbf{N}^{\mathrm{T}}(+1)\mathbf{v}^1(x,y) = 0 \text{ on } \omega^2, \\ \mathbf{N}^{\mathrm{T}}(-1)\mathbf{v}^3(x,y) = 0 \text{ on } \omega^2, \end{array} \right. \tag{21}$$

where the sub-spaces $\mathscr{U}^i(\omega^i)$, $V^i(\omega^i)$ were defined earlier in Eqs. (16), (17) and (18), while the matrices C^i were defined in Eq. (20).

Thus, the basic steps of the proposed methodology are

1. To compute the matrices C^i defined in Eq. (20) for a given order p. Observe that the matrices C^i are independent of the geometry of the MEMS device, and can therefore be pre-computed, where the height parameter H is treated symbolically during the computation.
2. Then, the 2-D coupled problem posed in Eq. (21) is solved over the 2-D region ω^i surrounding the devices, for a chosen value of H.
3. Finally, the 3-D solution is recovered using Eq. (15).
4. Further, 3-D charges, forces, etc. may be computed directly from the solution vectors $\mathbf{u}^i(x,y)$ (as discussed below).

Observe that the variational equation described in Eq. (21) when translated to a strong formulation [19] is of the simple form:

$$\mathbf{A}^i \nabla^2 \mathbf{u}^i + \mathbf{B}^i \mathbf{u}^i = 0 \text{ in } \omega^i, \tag{22}$$

where the coefficients are constant matrices, derivable from the matrices C^i. This is a simple 2-D partial equation involving vector fields $\mathbf{u}^i$. Any 2-D computational strategy may be used to solve this equation. In this paper, we use the finite-element method to solve Eq. (21) since the weak formulation is ideally suited for FEA.

2.4. Computing 3-D charges

Once the vector fields $\mathbf{u}^i$ are computed, the problem of computing the charge associated with the 3-D structure is now addressed. First consider the charge on the 3-D device D^v. By definition we have [23]

$$Q^v = \varepsilon_0 \int_{\partial D^v} \nabla U . \mathbf{n} \, \mathrm{d}\Gamma.$$

The charge arises from three contributions: (1) charge on the bottom of the device, i.e., $z=-H$ that can be computed from U^1, i.e., from $\mathbf{u}^1$, (2) charge on the side surfaces $z=-H\ldots H$ that can be computed from U^2, i.e., from $\mathbf{u}^2$, and finally (3) charge on the top of the device $z=H$ that can be computed from U^3, i.e., from $\mathbf{u}^3$:

$$Q^v=\varepsilon_0\left(\int_{d^v(-H)}\nabla U^1.\mathbf{n}\,\mathrm{d}\omega+\int_{\gamma^v}\int_{-H}^{H}\nabla U^2.\mathbf{n}\,\mathrm{d}z\,\mathrm{d}\gamma+\int_{d^v(H)}\nabla U^3.\mathbf{n}\,\mathrm{d}\omega\right).$$

Substituting for the gradients from Eq. (19), we have

$$Q^v=\varepsilon_0\left(\int_{d^v}\frac{\partial U^1}{\partial z}\,\mathrm{d}\omega+\int_{\gamma^v}\int_{-H}^{H}(U^2_{,x}n_x+U^2_{,y}n_y)\,\mathrm{d}z\,\mathrm{d}\gamma+\int_{d^v}\frac{\partial U^3}{\partial z}\,\mathrm{d}\omega\right).$$

Exploiting the representation of Eq. (15):

$$Q^v=\varepsilon_0\begin{pmatrix}\frac{1}{J^1}\int_{d^v}\mathbf{N}^{\mathrm{T}}_{,\xi}(+1)\mathbf{u}^1\,\mathrm{d}\omega\\ +J^2\int_{\gamma^v}(\bar{\mathbf{N}}^{\mathrm{T}}\mathbf{u}^2_{,x}n_x+\bar{\mathbf{N}}^{\mathrm{T}}\mathbf{u}^2_{,y}n_y)\,\mathrm{d}\gamma\\ -\frac{1}{J^3}\int_{d^v}\mathbf{N}^{\mathrm{T}}_{,\xi}(-1)\mathbf{u}^3\,\mathrm{d}\omega\end{pmatrix},$$

$$\bar{\mathbf{N}}\equiv\int_{-1}^{1}\mathbf{N}(\xi)\,\mathrm{d}\xi. \tag{23}$$

Thus the 3-D charges can be recovered directly from the 2-D fields $\mathbf{u}^i$. Similarly, one can compute the force on the 3-D device D^v from the 2-D fields $\mathbf{u}^i$.

2.5. Choice of shape functions $N_j(\xi)$

The results summarized in the previous section are valid for any set of linearly independent functions $N(\xi)$. Such functions include piece-wise polynomials, Lagrange polynomials and hierarchical polynomials. From a computational perspective, however, the objective is to choose a set that:

- for a given order p permits rapid computation of the C^i matrices defined in Eq. (20),
- for an increase in p, permits an easy update of the matrices. (Such updates are often necessary either during accuracy improvements or when the height of the MEMS devices is modified during design explorations.)

The hierarchical shape functions are the only ones that meet the above requirements [24]. Indeed, the following set of hierarchical functions has been shown to have robust properties, and is used in this work:

$$N_1(\xi)=(1-\xi)/2;$$
$$N_2(\xi)=(1+\xi)/2;$$
$$N_j(\xi)=\frac{P_j(\xi)-P_{j-2}(\xi)}{\sqrt{2(2j-3)}};\quad j\geqslant 3 \tag{24}$$

where $P_j(\xi)$ are the Legendre polynomials given by

$$P_1(\xi)=1;$$
$$P_2(\xi)=\xi;$$
$$P_j(\xi)=\frac{(2j-3)\xi P_{j-1}(\xi)-(j-2)P_{j-2}(\xi)}{j-1};\quad j\geqslant 3.$$

The first five functions $N_j(\xi)$ are plotted in Fig. 4.

Observe that with the above choice the middle term in Eq. (17) simplifies to $u_1^2(x,y)=u_2^2(x,y)=\hat{v}^\alpha$ on $\partial d^\alpha(\xi)$ and $u_i^2(x,y)=0$ on $\partial d^\alpha(\xi)$.

2.6. Implementation issues

Finally, we address certain implementation issues. As stated earlier, we use the finite-element method to solve Eq. (21) since the weak formulation is ideally suited for FEA. Yet another reason for choosing the finite-element method is that it will be convenient later on to couple 2-D structural mechanics with the proposed 2-D electrostatics formulation.

In particular, in all the numerical experiments below, we have employed a commercially available finite-element software package FEMLAB (version 3.2) [12] to solve the 3-D and 2-D reduced problems. As is well known, when FEA is used for modeling open-space problems, one must address the problem of boundary conditions at infinity. Many well-known techniques exist [25], and we have chosen the simplest, that of creating a large bounding box and setting the boundary conditions on the surface of this box to zero.

2.7. Modeling levitation

The presence of a ground plane in comb drives can lead to levitation in that the uncharged movable fingers will tend to move away from the ground plane. Consequently, the simple decomposition of the 3-D region of interest into

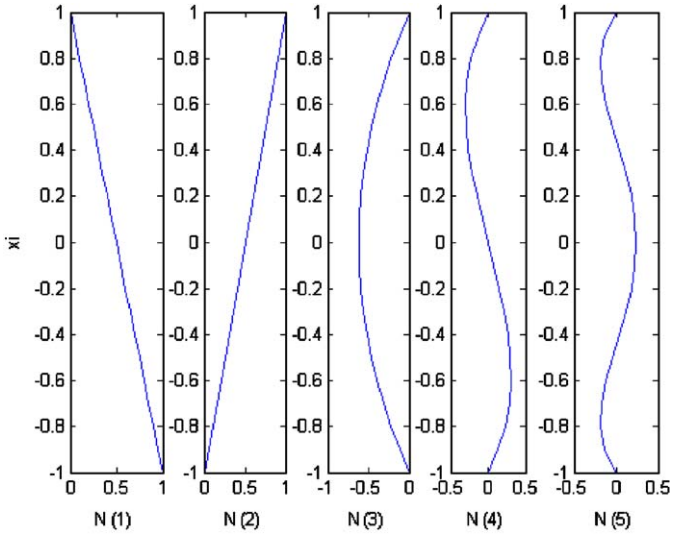

Fig. 4. The first five functions described in Eq. (24).

three regions (see the first paragraph of Section 2), each of which is a swept region does not hold any more. Further, the levitation (offset) will depend on the applied voltage and resisting forces, and is not known a priori.

One approach to model levitation within the proposed dimensional reduction strategy is to decompose the 3-D region of interest into *five* regions; the *two additional* regions have a thickness equal to the (unknown) levitation distance. Each of the five regions is a swept region, so the proposed framework applies. Thus, one defines five unknown fields as opposed to three; with appropriate functional space approximation similar to the ones used in the paper, one arrives at a coupled weak formulation with one of the parameters as levitation distance. Initially, one can assume that the levitation distance is zero, predict the levitation force, update the levitation distance and repeat (formulated as a weakly coupled multi-physics problem). This work has not yet been implemented.

3. Numerical examples

We are now ready to solve the dimensionally reduced problem posed in Eq. (21) and compare the results to the solution from the full 3-D problem of Eq. (1) and classical 2-D problem of Eq. (2).

Example 1. The first example is that of a parallel plate problem consisting of two plates, each of width 10 μm, length 100 μm, variable height $2H$ and distance 20 μm apart. One plate is grounded while the other is at 1 V. We assume that the plates are enclosed in a space that is open in all directions except for a grounding plane at 50 μm below the device. The objective is to compute the charge on the positively charged plate.

Fig. 5 illustrates the ratio of the computed 3-D to 2-D charge using both classical 2-D per Eq. (2) and proposed 2-D per Eq. (21). Classical 2-D grossly under-predicts the charge when the plate height is comparable to the gap, i.e., when fringing effects cannot be neglected. The proposed method performs well through the entire range of height to gap ratio since 3-D fringing is fully accounted for.

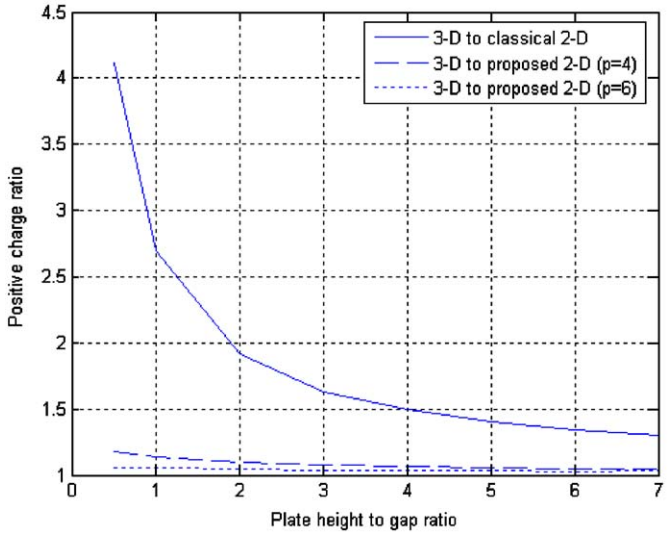

Fig. 5. Ratio of computed positive charge.

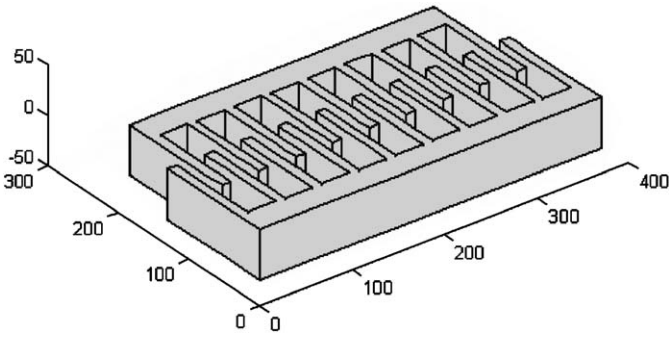

Fig. 6. A nine-tooth comb drive.

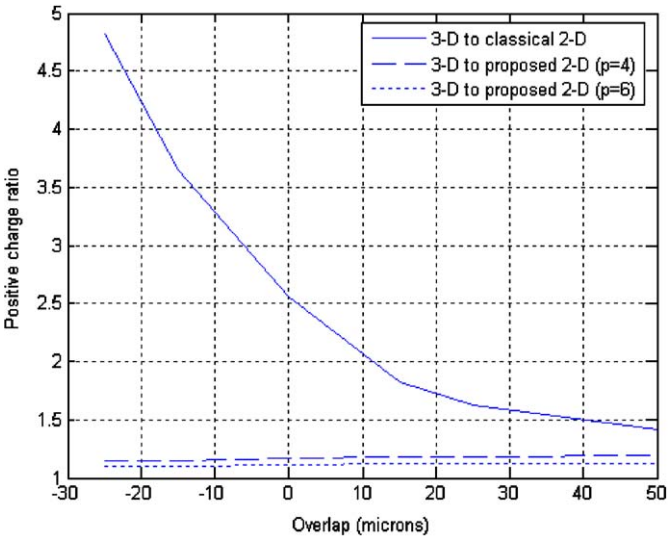

Fig. 7. Ratio of computed positive charge.

Example 2. The next example we consider is that of a comb illustrated in Fig. 6. The parameters of the comb drive are as follows:

- teeth thickness and gap: 10 μm; height: 50 μm,
- teeth length: 100 μm,
- number of teeth: 10 and 9,
- boundary conditions: insulated in (x, y) directions at 150 μm away from the device, grounded on a plane 50 μm below, and open above,
- the larger of the two combs is assigned a positive voltage, while the other is set at ground.

Here the geometry of the comb drive is kept constant, while the overlap between the two combs is varied. Fig. 7 illustrates the ratio of charges on the positive comb as a function of the overlap. Again, one can observe the superiority of the proposed 2-D method over classical 2-D method. Typical CPU time for simulating the comb

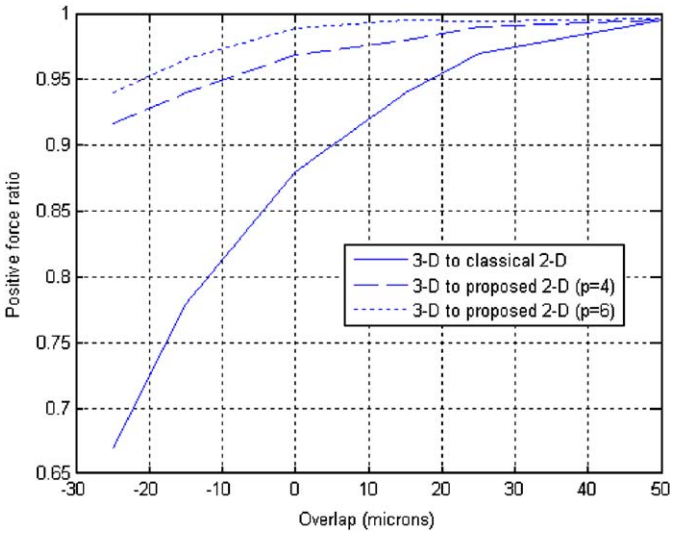

Fig. 8. Ratio of computed positive charge.

drive on a Pentium-4 (2.4 GHz) equipped with 1 Gbyte of memory are as follows:

- classical 2-D: 1.1 s,
- proposed 2-D ($p = 4$): 9.2 s,
- proposed 2-D ($p = 6$): 14.3 s,
- full 3-D: 68 s.

The computational cost for the proposed method is higher than the classical 2-D and much lower than full 3-D simulation as expected. Not accounted for above is the cost involved in constructing the 3-D geometry.

The ratio of forces on the positively charged plate is illustrated in Fig. 8. Once again the superiority of the proposed 2-D method is evident.

4. Conclusions

We have proposed here a novel method for simulating 3-D electrostatic problems through a reduced 2-D model that fully accounts for 3-D fringing. Thus, one need not construct 3-D geometry or surface/volume mesh in order to extract 3-D behavioral characteristics of MEMS device. Further, as demonstrated through theory and experiments, the accuracy of the 2-D model can be controlled through a dimensional reduction parameter. An immediate extension of this work is multi-physics coupling where the 3-D electrostatic simulation is to be coupled with the structural simulation. Other extensions include modeling MEMS devices whose components are of varying heights. It is eventual objective of this project to be able to fully simulate the physical behavior of MEMS devices directly from 2-D CIF or other popular 2-D MEMS formats.

References

[1] Ye W, Mukherjee S, MacDonald NC. Optimal shape design of an electrostatic comb drive in microelectromechanical systems. J Microelectromech Systems 1998;7(1):16–26.
[2] Ye W, Mukherjee S. Optimal shape design of three-dimensional MEMS with applications to electrostatic comb drives. Int J Numer Meth Eng 1999;45:175–94.
[3] Jensen BDMS, Miller S, Kurabayashi K, Allen JJ. Shaped comb fingers for tailored electromechanical restoring force. J Microelectromech Systems 2003;12(3):373–83.
[4] Collenz A, Bona FD, Gugliotta A, Soma A. Large deflections of microbeams under electrostatic loads. J Micromech Microeng 2004;14:365–73.
[5] Li G, Aluru NR. A Lagrangian approach for electrostatic analysis of deformable conductors. J Microelectromech Systems 2002;11(3):245–54.
[6] Li G, Aluru NR. Efficient mixed-domain analysis of electrostatic MEMS. IEEE Trans Comput Aided Des Integr Circuits Systems 2003;22(9):1228–42.
[7] Shrivastava V, Aluru NR, Mukherjee S. Numerical analysis of 3D electrostatics of deformable conductors using a Lagrangian approach. Eng Anal Boundary Elements 2004;28:583–91.
[8] Han JS, Rudnyi EB, Korvink JG. Efficient optimization of transient dynamic problems in MEMS devices using model order reduction. J Micromech Microeng 2005;15:822–32.
[9] Hung ES, Senturia SD. Generating efficient dynamical models for microelectromechanical systems from a few finite-element simulation runs. IEEE J Microelectromech Systems 1999;8(3):280–9.
[10] Lienemann J, Rudnyi EB, Korvink JG. MST MEMS model order reduction: requirements and benchmarks. Linear Algebra Appl 2006;415(2–3):469–98.
[11] ANSYS, ANSYS Multiphysics; www.ansys.com, 2005.
[12] COMSOL, FEMLAB 3.1; www.comsol.com, 2005.
[13] Coventor, CoSolve-EM; www.coventor.com, 2005.
[14] Ong ET, Lee KH, Lim KM. A fast algorithm for three-dimensional electrostatics analysis: fast Fourier transform on multipoles. Int J Numer Methods Eng 2004;61:633–56.
[15] Liao Y-S, Chyuan S-W, Chen J-T. An alternatively efficient method (DBEM) for simulating the electrostatic field and levitating force of a MEMS combdrive. J Micromech Microeng 2004;14:1258–69.
[16] Shrivastava V, Aluru NR. A fast boundary cloud method for 3D exterior electrostatic analysis. Int J Numer Methods Eng 2004;59:2019–46.
[17] Bao Z, Mukherjee S. Electrostatic BEM for MEMS with thin conducting plates and shells. Eng Anal Boundary Elements 2004;28:1427–35.
[18] Becker AA. The boundary element method. New York: McGraw Hill; 1992.
[19] Reddy DB. Introductory functional analysis with applications to boundary value problems and finite elements. Texts in applied mathematics, vol. 27. New York: Springer; 1997.
[20] Vasilev VV. Modern conceptions of plate theory. Composite Struct 2000;48:39–48.
[21] Reissner E. Reflections on the theory of elastic plates. Appl Mech Rev 1985;38:1453–64.
[22] Piltner R. The derivation of a thick and thin plate formulation without ad hoc assumptions. J Elast 1992;29:133–73.
[23] Ida N. Engineering electromagnetics. New York: Springer; 2000.
[24] Zienkiewicz OC, Gagom JP, Kelly DW. The hierarchical concept in finite element analysis. Comput Struct 1983;16(1–4):53–65.
[25] Webb JP. Application of the finite element method of electromagnetic and electrical topics. Rep Prog Phys 1995;58:1673–712.